Available online at www.sciencedirect.com
ScienceDirect
International Journal of Thermal Sciences 46 (2007) 1112–1125
International Journal of Thermal Sciences
www.elsevier.com/locate/ijts

Measurement of local liquid temperature using micro-thermocouple in subcooled flow boiling

Seong-Jin Kim [a], Goon-Cherl Park [b,*]

[a] *Department of Nuclear Engineering, Seoul National University, Nuclear Thermal Hydraulics Engineering Laboratory, 31-205, San 56-1, Sillim-dong, Kwanak-gu, Seoul, 151-742, South Korea*
[b] *Department of Nuclear Engineering, Seoul National University, Nuclear Thermal Hydraulics Engineering Laboratory, 32-213, San 56-1, Sillim-dong, Kwanak-gu, Seoul, 151-742, South Korea*

Received 31 July 2006; received in revised form 22 March 2007; accepted 23 March 2007

Abstract

In this paper, the developed algorithm was described, which can discriminate the local phase temperature in the two-phase flow measured by a self-designed micro-thermocouple with an outer diameter of 12.7 μm. The algorithm used to calculate the temperature of each phase was based on the response time of the micro-thermocouple and the exponential regression method. This algorithm was verified by conducting experiments with an optical chopper and a laser. It was shown that the more accurate temperatures were measured, when the newly proposed algorithm was used. Moreover, this algorithm was applied to the measurement of the liquid temperature in subcooled flow boiling. The measured liquid temperatures in subcooled flow boiling were used to assess the capability of the CFX-4.2 code, additionally.

Keywords: Micro-thermocouple; Optical chopper; Exponential regression method; CFX-4.2

1. Introduction

In the case of subcooled boiling, thermal non-equilibrium phases, vapor and liquid phases coexist, and bubble condensation at the bubble-liquid interface is the major mechanism of heat transfer. The measurements of the phase temperatures play an important role in the determination of the interfacial heat transfer coefficient for bubble condensation, which is required to constitute the governing equation for energy transfer. Thus, various sensors and algorithms designed to accurately measure the fast changes in temperature caused by phase transfer have been developed using a micro-sized sensor to measure temperatures. The temperature distribution in the case of subcooled boiling was measured by Jiji and Clark [1] and Walmet and Staub [2]. However, they did not provided any reliable statistical information on the distribution of the temperature between the liquid and vapor phases. Delhaye et al. [3] used the statistical information provided by the Probability Density Function (PDF) of temperatures to determine the void fraction and temperatures in the case of subcooled boiling using 25 and 20 μm micro-thermocouples. Also, Roy et al. [4–7] measured the temperatures of the liquid and vapor phases with the PDF method using R-113 as the working fluid. The micro-thermocouples used in these studies were of the complex type, with a disk-shaped junction being used to fabricate them. Nakamura et al. [8] used a copper-constantan thermocouple with a diameter of 0.1 mm to investigate the fluid flow and local heat transfer around a cube mounted on the wall of a plane. Recently, Warrier et al. [9] used a micro-thermocouple with a diameter of 0.25 mm to measure the liquid temperature. However, the method that they used to measure the liquid temperature was deficient, in that it involved recording the lowest temperature observed during the measurement period.

Studied involving the measurement of the phase temperatures have generally been performed using a micro-thermocouple, in order to obtain a fast time constant. Among these studies, the PDF method and statistically ensemble averaging method were widely used for the statistical analysis of the mea-

* Corresponding author.
E-mail addresses: nannaya2@snu.ac.kr (S.-J. Kim), parkgc@snu.ac.kr (G.-C. Park).

1290-0729/$ – see front matter
doi:10.1016/j.ijthermalsci.2007.03.012

Nomenclature

a	coefficient of an exponential function	
A	area	m^2
ATD	averaged temperature displacement	K
b	coefficient of an exponential function	
Bi	Biot number	
c	coefficient of an exponential function	
C	correction constant	K
C_p	specific heat	J/kg K
h	convection heat transfer coefficient	W/m^2 K
I, Y	coefficient matrix	
l	time interval to calculate averaged temperature	s
L	multiplier of parameter l	
s	time interval to calculate displacement of the averaging temperature	s
S	multiplier of parameter s	
STD	standard deviation	
t	time	s
Δt	time intervals	s
T	temperature	°C
V	volume	m^3

Greek letters

α, β, γ	coefficients of exponential function	
ρ	density	kg/m^3
τ	time constant	s
Λ	coefficient matrix	

Subscripts

0	initial
1ϕ	single phase
air	air
bubble	bubble
crit	criterion
exp	experiment
i	ith position
J	junction
k	kth index
m	medium
max	maximal
min	minimal
resolution	resolution

sured temperatures. However, when a fast response time is required, such as in the case of subcooled boiling, it proved to be difficult to obtain accurate value for the temperature of each phase with the PDF and ensemble averaging methods.

The objective of this study is to develop an algorithm which can provide a more accurate estimate of the phase temperature using a self fabricated micro-thermocouple (12.7 μm, K-type). The applicability of the developed algorithm is verified by conducting an experiment with an optical chopper. The experimental results for the liquid temperature estimated by the developed algorithm are compared with CFX-4.2 to assess CFX-code's capability.

2. Algorithm used to estimate the phase temperature

The lumped energy balance equation corresponding to the hot junction of the micro-thermocouple can be written in the form of Eq. (1). In this study, the Biot number is less than 0.1, and heat transfer effects of conduction and radiation can be neglected.

$$\frac{\mathrm{d}T_J}{\mathrm{d}t} = -\frac{t}{\tau}(T_J - T_m) \tag{1}$$

Therefore, the lumped temperature becomes:

$$T_J(t) = T_m + \left[T_J(0) - T_m\right]e^{-t/\tau} \tag{2}$$

where $T_J(0)$ refers to be the initial temperature of micro-thermocouple and τ is a time constant defined as:

$$\tau = \frac{\rho_J V_J C_{pJ}}{h_m A_J} \tag{3}$$

Here, ρ_J, V_J and C_{pJ} are the density, volume and specific heat of the junction, respectively, A_J is the surface area of the junction exposed to the fluid and surroundings and h_m is the convection heat transfer coefficient at the junction with respect to the medium passing through the junction. The characteristic curve has an exponential form, which is dependent on the time constant in Eq. (3). Therefore, the temperatures of the surrounding elements passing the junction, such as air bubbles and water, can be measured using this characteristic of the heat transfer at the junction.

The algorithm is developed using these characteristics and consists of two steps. The first step is to discriminate the phases and the second step is to estimate the phase temperatures. The process of the developed algorithm is shown in Fig. 1. Each procedure is explained in detail in the following sections.

2.1. Discrimination of phases

In the first step of the developed algorithm, the phase between the vapor and liquid in the raw data obtained from the micro-thermocouple was discriminated to find the characteristic temperature curve piece by piece. The temperature at the hot junction begins to change at the moment when the hot junction comes into contacts with the other phase, assuming that the wetting effects of the micro-thermocouple can be neglected. The gradient of the temperature variation has a maximum or minimum value at the time-point when the medium at the hot junction is changed due to its exponential characteristics. Taking into consideration the effects of noise and fluctuation, the averaged temperature displacement (ATD) of the temperature change can be defined and calculated at each time point, $i + S/2$, as:

$$\mathrm{ATD}_{i+S/2} = \frac{\sum_{k=(i+S)}^{k=(i+S)+L} T_k - \sum_{k=i}^{k=i+L} T_k}{L} \tag{4}$$

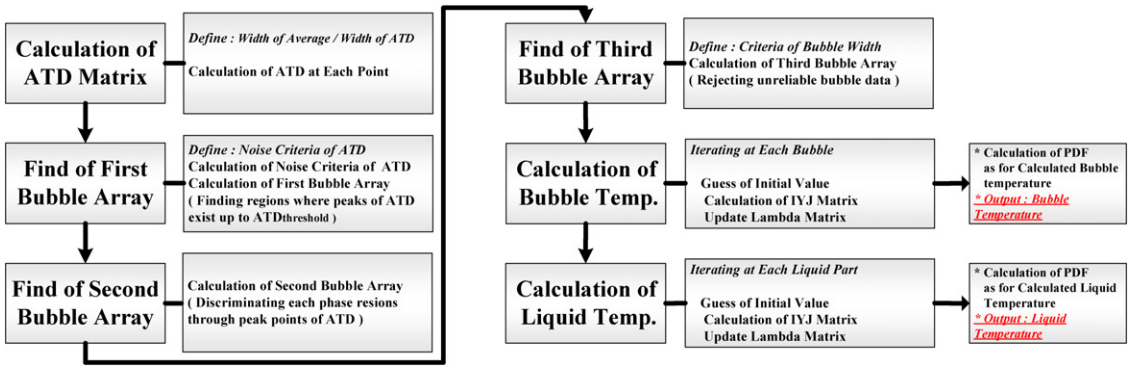

Fig. 1. Flow chart of the developed algorithm.

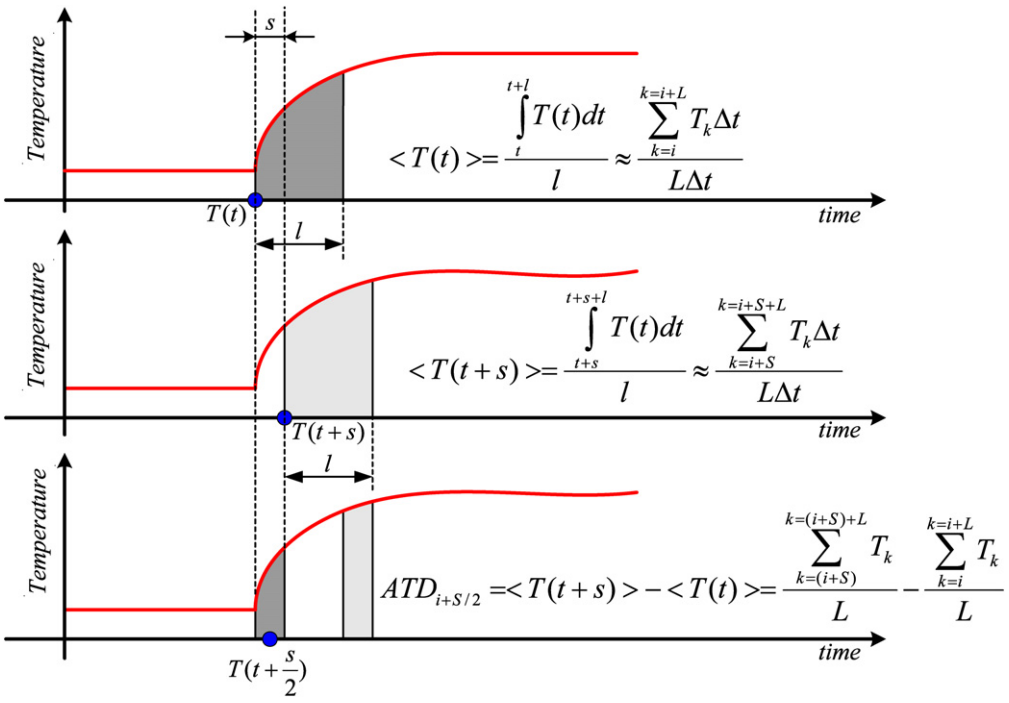

Fig. 2. Averaged temperature displacement.

where l is the time interval used to calculate the averaged temperature. s is the time interval used to calculate the displacement of the averaging temperature at each time-point as shown in Fig. 2, where t, l and s mean $i\Delta t$, $L\Delta t$ and $S\Delta t$, respectively. $1/\Delta t$ is the sampling rate of the data acquisition system. These two parameters play a role in reducing the effects of noise in the actual micro-thermocouple signal.

L is designed to reduce the effects caused by resolution of the data acquisition system and noises. The value of L is determined so as to satisfy Eq. (5).

$$\frac{\mathrm{STD}(\langle T(t)\rangle)}{\mathrm{STD}(T(t))} < 0.1 \tag{5}$$

where STD is the standard deviation and L plays the role of to reducing the standard deviation to 10% of the original raw data.

S is used to take into consideration the time constant of the micro-thermocouple, noisy and fluctuating temperature signal when the ATD is calculated. Assuming that the displacement between the first and second time points must be higher than the STD of noisy and fluctuating temperature signal, in order to discriminate the temperature change, the value of S must satisfy the following equation:

$$\left|T(t_0+s)-T(t_0)\right| = \left|\Delta T e^{-t_0/\tau}\left(e^{-s/\tau}-1\right)\right| \geqslant \frac{1}{2}C_{\exp} \tag{6}$$

where $C_{\exp}$ is a correction constant which is determined experimentally using the relation as:

$$C_{\exp} = \mathrm{Max}\left(|\Delta T_{1\phi}|, |2\Delta T_{\mathrm{resolution}}|\right) \tag{7}$$

Here, $\Delta T_{1\phi}$ refers to the temperature width of the measured signal of each phase at the steady state and $\Delta T_{\mathrm{resolution}}$ refers to the temperature resolution, which is dependent on the data acquisition system.

Assuming $\min(|\Delta T|) = 4|C_{\exp}|$ for the exponential regression method, then the next inequality equation must satisfy the following relations

$$\left|e^{-s/\tau}-1\right| \geqslant \frac{\mathrm{STD}(C_{\exp})}{|\Delta T e^{-\frac{t_0}{\tau}}|} \geqslant \frac{\mathrm{STD}(C_{\exp})}{|\Delta T|} \cong \frac{\mathrm{STD}(C_{\exp})}{|4C_{\exp}|} \tag{8}$$

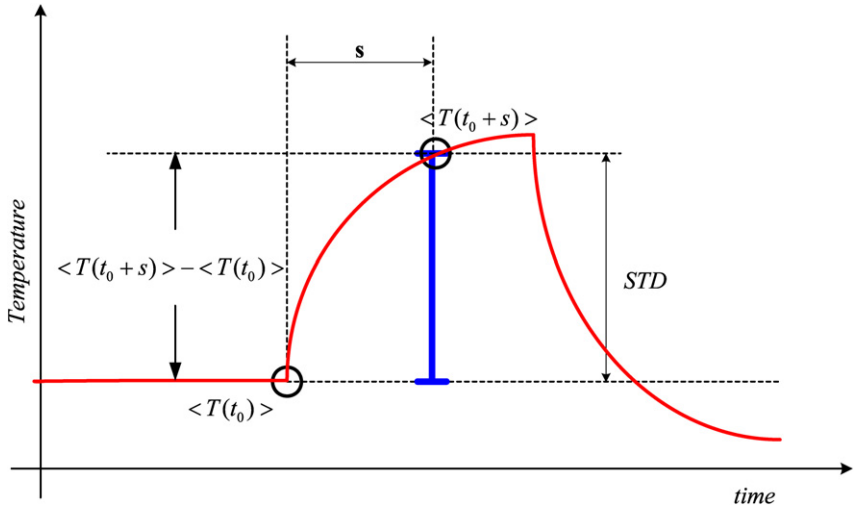

Fig. 3. Determination of S-value.

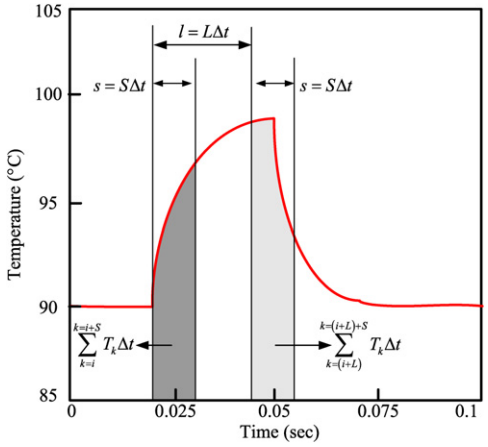

Fig. 4. Concept of the ATD calculation.

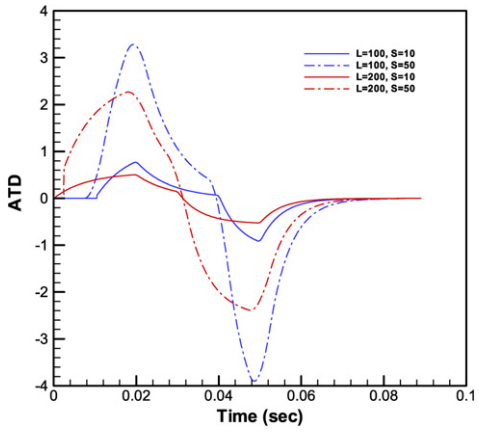

Fig. 5. Sensitivity analysis of ATD parameters.

The value of S must satisfy the following equation

$$s = (S\Delta f) \geqslant 0.0125\tau \tag{9}$$

Fig. 3 shows the meaning of S which is that the value of $s(= S\Delta f)$ must be greater than 1.25% of the time constant of the micro-thermocouple. S is used to average the temperatures over the short time interval, while taking into consideration the fluctuations of the temperature signal with noise. Since the absolute magnitude of the ATD decreases as the value of S increases, the ATD offers the advantage of having a smooth shape. However, distinguishing between true and false ATDs generated by noises becomes more difficult.

If a single bubble passes through the junction of the micro-thermocouple, the ATD has a maximum value at the time when the bubble starts to pass through the junction and a minimum value at the time when the bubble has passed through the junction completely, as shown in Figs. 4 and 5. The time points corresponding to the maximum or minimum value are independent of the values of S and L as shown in Fig. 5.

Although the temperature at the hot junction is fixed, calculated values of the maximum or minimum points of the ATD can nevertheless be incorrect due to the noise and the fluctuation of the medium. Thus, the threshold should be designed so to correctly discriminate between the vapor and liquid temperatures. The value of this threshold is proportional to S and inversely proportional to L. Thus, it can be determined as,

$$\mathrm{ATD}_{\mathrm{threshold}} = C_{\exp}\frac{S}{L} \tag{10}$$

This ATD, which is the primary information concerning the phases, includes the time region containing areas where extreme values of the ATD exist satisfying the threshold conditions of the ATD.

In the next step, the start and end time points of the phase changes at the junction should be determined. However, the micro-thermocouple may not have enough time to detect the fast change in temperature if the distance between successive bubbles is too short. The detection of bubbles may be rejected by the ATD threshold condition, which was been described in the previous step. Since this can cause actual bubbles to be neglected, backward and forward searching procedures are implemented in this algorithm, in order to obtain the necessary information on bubbles, which were overloaded under the ATD threshold condition. It is possible that the start position of the $(n+1)$th bubble can be situated at the end position of the nth

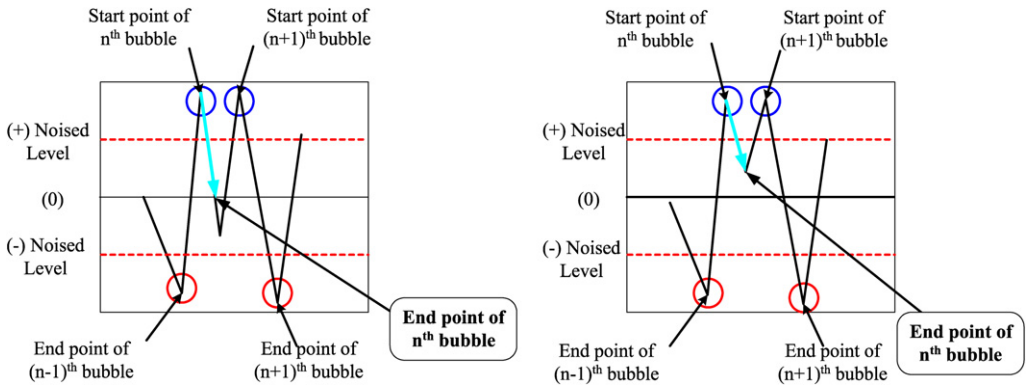

Fig. 6. Forward searching procedures.

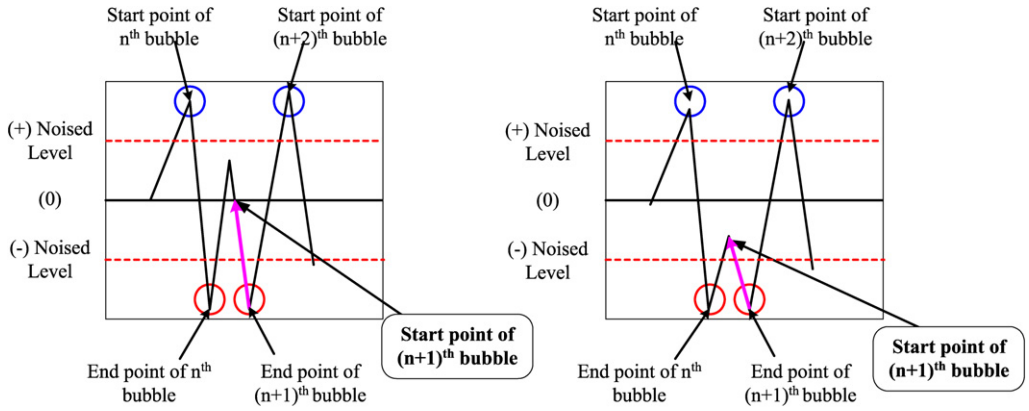

Fig. 7. Backward searching procedures.

bubble in the ATD information determined by ATD threshold condition, as shown in Fig. 6. This is possible because the magnitude of the ATD at the end position of the nth bubble is less than $\mathrm{ATD}_{\mathrm{threshold}}$. There are two possible cases, as shown in Fig. 6. The first case is where the end position of the nth bubble is positioned in the negative ATD region passing through the 0 ATD value, as shown in Fig. 6(a). In this case, the end position of the nth bubble is taken to be situated at the point where the ATD reaches zero by forward searching. The second case is where the ATD does not pass through the 0ATD value shown in Fig. 6(b). In this case, the end position of the nth bubble is taken to be situated at the point where the ATD reaches a minimum, between the start position of the nth bubble and the start position of $(n+1)$th bubble by forward searching. Thus, the end position of the nth bubble can be found by forward searching from start position of the nth bubble.

On the other hand, the start position of the $(n+1)$th bubble can be found by backward searching from the end position of the $(n+1)$th bubble. There are two possible cases here, which are similar to those in the forward searching procedures. These procedures are shown in Fig. 7.

As the final step of in the discrimination of each phase section, the criterion of the bubble width is applied to the time information, which successfully satisfies the above sequences. The criterion of the bubble width condition is used to remove the non-physical data corresponding to the bubble residence time, which can be calculated using the noisy signal and the averaging process.

2.2. Determination of phase temperature

The bubble temperature is determined based on the characteristics of the temperature measured by the micro-thermocouple and the information used to discriminate the phases, which was referred to in the previous section. It is assumed that the temperature change occurs along the exponential curve, as described in Eq. (2), so it can be rewritten as follows

$$T(t) = \alpha + \beta e^{\gamma t} \tag{11}$$

When the temperature is increased by the bubble, T is the temperature at the junction, and α and β refer to $T_{\max} = (T_{\mathrm{bubble}})$ and $T_{\max} - T_{\min} = (T_{\mathrm{bubble}} - T_{\mathrm{liquid}})$, respectively. When the temperature at the hot junction of the micro-thermocouple is decreased by the cold water, and α and β become T_{water} and $T_{\mathrm{liquid}} - T_{\mathrm{bubble}}$, respectively. $-1/\gamma$ is the time constant of the micro-thermocouple.

If the residence time at the hot junction of the micro-thermocouple is smaller than the time constant or its magnitude is of a similar orders, the hot-junction will not reach the temperature of the exponential curve. Thus, the temperature data is only a part of the entire exponential curve. That is, the convergent temperature can be determined by the exponential regression method, which was proposed by Langer [10]. The

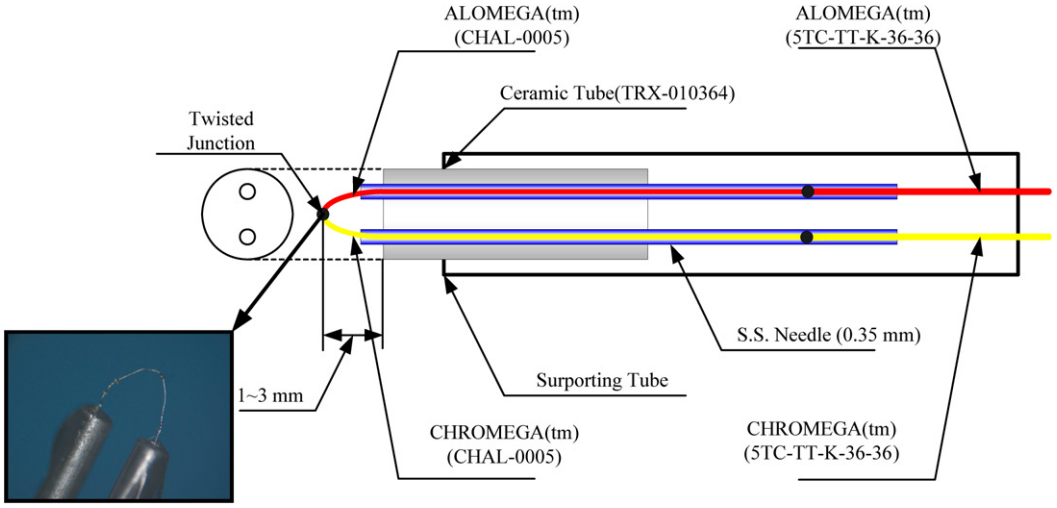

Fig. 8. Self designed and fabricated micro-thermocouple.

procedures used in the exponential regression method can be summarized as follows.

Let y_i and $S(a,b,c)$ be given by

$$y_i = \alpha + \beta e^{\gamma x_i} \tag{12}$$

$$S(a,b,c) = \sum_{i=1}^{n} \left[y_i - \left(a + b e^{c x_i} \right) \right]^2 \tag{13}$$

where, y_i are the measured values, which have the form of an exponential function at x_i such as temperatures, and $a + be^{cx_i}$ is the regressed function to be found. Therefore, $S(a,b,c)$ refers to the residual between the measured values and the regressed values. Neglecting the high order terms of the Taylor expansion as for c at x_i, Eq. (13) can be expressed as

$$\Lambda = I^{-1} Y \tag{14}$$

where each matrix is defined as follows,

$$\Lambda = \begin{pmatrix} a(c_0) \\ b(c_0) \\ b(c_0)c_0 \end{pmatrix} \tag{15}$$

$$Y = \begin{pmatrix} \sum_{i=1}^{n} y_i \\ \sum_{i=1}^{n} y_i e^{c_0 x_i} \\ \sum_{i=1}^{n} x_i y_i e^{c_0 x_i} \end{pmatrix} \tag{16}$$

$$I = \begin{pmatrix} n & \sum_{i=1}^{n} e^{c x_i} & \sum_{i=1}^{n} x_i e^{c x_i} \\ \sum_{i=1}^{n} e^{c x_i} & \sum_{i=1}^{n} e^{2c x_i} & \sum_{i=1}^{n} x_i e^{2c x_i} \\ \sum_{i=1}^{n} x_i e^{c x_i} & \sum_{i=1}^{n} x_i e^{2c x_i} & \sum_{i=1}^{n} x_i^2 e^{c x_i} \end{pmatrix} \tag{17}$$

The coefficients of Eq. (12) are updated by the repeating the calculation after guessing the initial values and, then, calculating the temperatures of the phases. Finally, each calculated temperature is used to build the probabilities of the temperature and to form the PDF.

3. Experiments

3.1. Experiments for verifying algorithm

3.1.1. Fabrication of micro-thermocouple

The micro-thermocouple manufactured in this study has an outer diameter of 12.7 μm and is shaped like a hot-wire type as shown in Fig. 8. The micro-thermocouple is fabricated using a couple made of alumel-chromel wire (K-type).

The hot junction is twisted and a ceramic tube electrically insulates each wire. A needle then supports each wire, in order to protect it against the fluctuations caused by the water and bubbles. The wire, which has an outer diameter of 12.7 μm, is extended using a read wire with an O.D. of 127 μm by pressing it into the needle and sealing it with epoxy. Each wire adjacent to the junction in the needle is fixed with epoxy.

3.1.2. Dynamic calibration

The dynamic calibration of the fabricated micro-thermocouple is performed using Argon-Ion laser beam and shutter as shown in Fig. 9. The developed algorithm was verified, by conducting various experiments using an optical chopper (Stanford Research Systems, Inc. Model SR540). The aim of this calibration is to find the time constant of the micro-thermocouple, which determines the response time of the micro-thermocouple. The camera shutter is alternately closed and opened so as to intermittently expose the heat source to the hot junction.

The ice-point device was used to make the cold junction's temperature the freezing point and the other thermocouple was used to know the temperature in the ice-point device, i.e., the temperature of the cold junction. The cold junction was made by 127 μm wires and connected to the hot junction. The composed devices to measure temperature are depicted in Fig. 10. Before the micro-thermocouple is used, the micro-thermocouple was calibrated in the iso-thermal box (Gemini 857/I, Isotech Co. Error ±0.05 °C) with RTD (Calibrated Pt 100 Probe, Error ±0.01 °C) as the reference temperature device. The uncertainty of the micro-thermocouple is ±0.1°C. When the compositions for measuring temperature are same to

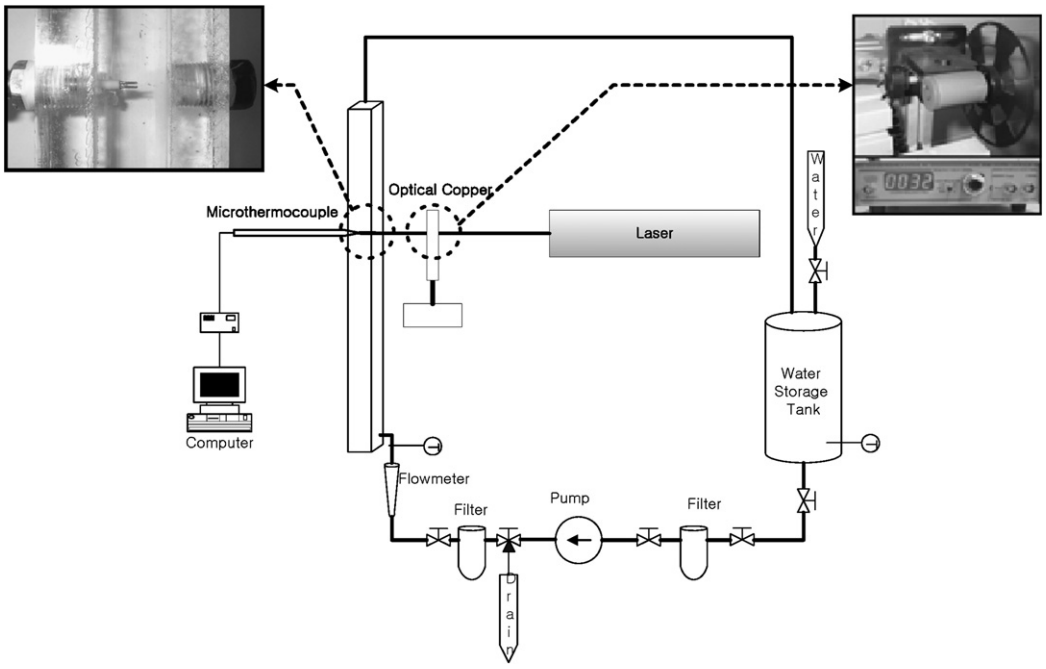

Fig. 9. Schematic diagram of experimental facility with optical chopper.

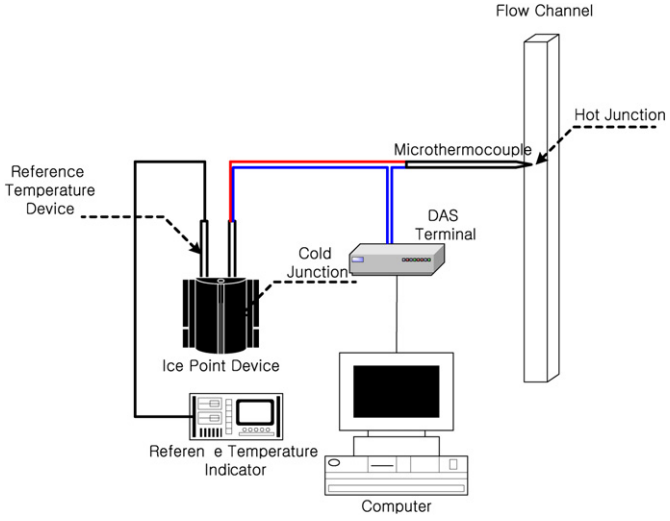

Fig. 10. Composed devices to measure temperature.

Table 1
Uncertainty of micro-thermocouple

Contents	Absolute uncertainty
Micro-thermocouple	±0.100 °C
DAS	±0.244 °C
Iso-thermal box	±0.050 °C
Reference temperature device	±0.010 °C

Table 2
Experimental cases

Experiments	Frequency of optical chopper (Hz)	Residence time (ms)
Case 1	32	15.625
Case 2	64	7.813
Case 3	128	3.906
Case 4	256	1.953

Fig. 10, the uncertainty in the measurement of the temperature is ±0.27 °C. The used uncertainty data are summarized in Table 1.

The calibration was performed using a flow rate of water of 0 to 1.2 m/s. The laser power was varied from 3 to 9 W. The laser power is varied in order to adjust the sudden differences in temperature at the hot junction. The beam is intercepted using the shutter and measurements are conducted when the shutter is repeatedly open and closed. The temperature data were acquired by means of an A/D board (DT3003-PGL) during a period of 2 seconds with of sampling rates of 300 kHz.

The experiments were conducted for the various conditions of liquid velocity and optical chopper frequency. Table 2 shows the four experimental cases with different optical chopper frequencies used for dynamic calibration. The role of the optical chopper is to intercept the heat emanating from the laser. The micro-thermocouple is subjected to thermal variation by adjusting the frequency of the optical chopper. The opening of the optical chopper, which allows the heat from the laser to pass, corresponds to a bubble, while the closing of the optical chopper, which cuts off the heat, corresponds to the relatively cold liquid phase. The frequency of the optical chopper is related to the residence time of the bubble at the hot junction. For example, when the frequency of the optical chopper is 256 Hz, the residence time becomes 1.953 ms as shown in Table 2. The temperature in the steady state is determined before and after the operation of the optical chopper, in the form of minimal and maximal temperatures, which are measured and are separately time-averaged in each case. Those values are used to transform the temperature into the PDF with and without the developed algorithm.

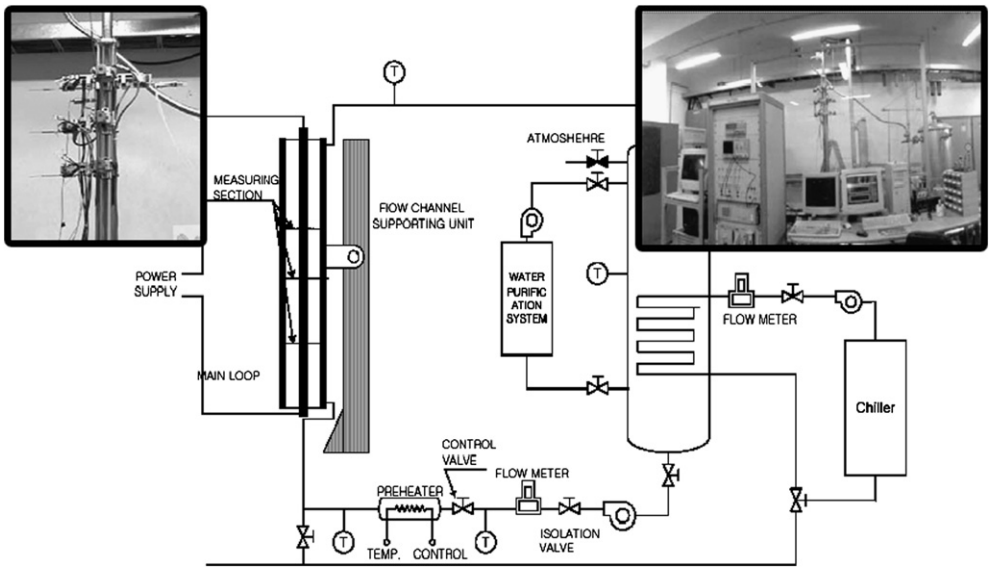

Fig. 11. Experimental apparatus used to measure the subcooled flow boiling.

Table 3
Experimental cases of the subcooled flow boiling

Case	Flow rate (LPM)	Liquid velocity (m/s)	Heat flux (kW/m^2)	Inlet subcooled degree (K)	Inlet pressure (MPa)
G1Q1	17.9	0.5729	96.695	20.655	0.11823
G2Q1	13.9	0.4449	96.695	23.320	0.12216
G2Q2			81.125	23.410	0.11875
G3Q3	10.0	0.3201	67.377	23.680	0.12473
G3G2			80.978	22.843	0.12430

3.2. Measurement of liquid temperature in subcooled boiling

The fabricated micro-thermocouple and the developed algorithm were used to measure the liquid temperature in a subcooled flow boiling experiment. Fig. 11 shows a schematic diagram of the flow boiling loop and a photograph of the measuring devices. The flow channel is a vertical concentric annulus with a length of 2.870 mm with the heated inner tube. The inner tube, which has an outer diameter of 19 mm is composed of a heated section and silver-soldered copper electrodes at both ends of the heated section. The heated section is a 1.870 mm long inconel 625 tube with a 1.5 mm wall thickness. This heated section is preceded and followed by 500 mm long and by 690 mm long, copper tubes, respectively. The outer tube is composed of Pyrex tube, so that visual observation or taking a photograph is possible, and stainless tubes with 32 mm inner diameter.

The inlet and outlet temperatures were measured by RTDs, which were calibrated within ± 0.2 K. The static pressure was measured at the inlet, outlet and measured point by DPI260 (Drug Co.) and the errors are ± 0.001 MPa. The mass flow rate was measured by a variable-area flow meter whose error is $\pm 5\%$. The micrometer was used to traverse the micro-thermocouple and it has the resolution of 1/100 mm.

The micro-thermocouple was installed at the position corresponding to $L/D_h = 125.4$, and the temperature was measured at 0.6, 0.7, 0.9, 1.3, 1.8, 2.4, 3.1 and 3.8 mm from the heated wall, radially. The experimental conditions are listed in Table 3. The signal from the micro-thermocouple is monitored using an A/D-board (DT3003-PGL) for a period of 12 seconds at sampling rates of 167 kHz.

The results of measuring local liquid temperature using micro-thermocouple were compared with CFX-4.2.

4. Results

4.1. Experiments conducted to verify the algorithm

Figs. 12 and 13 show the results of the dynamic calibration. Figs. 12 and 13 show the time constant distributions when the hot-junction is exposed to the heat source due to the sudden opening of the shutter and when the shutter suddenly intercepts the heat source, respectively. The fabricated micro-thermocouple has a time constant of about 2–4 ms, except that the water is in the stationary state. The results show that the fabricated micro-thermocouple has a fast time constant corresponding to the values reported in previous studies (1991, 1993, 1994 and 1995), even though the device is manufactured in this study was much easier to fabricate. From the results, it is noted that the fabricated micro-thermocouple can measure the temperature of both the bubbles and the liquid even when the residence times of each phase at the junction are as low as several milliseconds. Also, the results show that the time constants have a similar value for various conditions, and which is independent on the laser power. Thus, the time constant is almost unchanged by the difference in the temperature of the phases.

Fig. 14 shows the measured temperature and different phase regime distinguished by the developed algorithm. The long-dashed and dash-dotted lines correspond to periods of heating by the laser and the cooling by liquid, respectively. The solid lines indicate the raw data temperatures. The areas surrounded by the long-dashed line in Fig. 14(a). refer to the periods of the time during which the temperature is increased by the heat

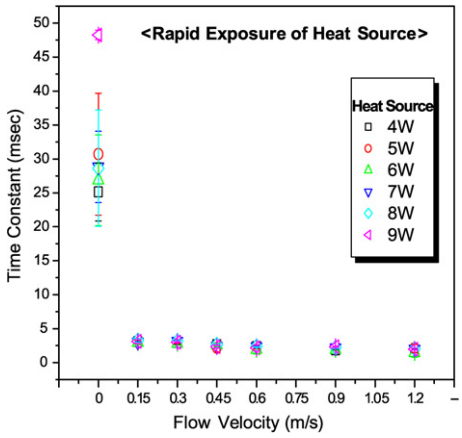

Fig. 12. Time constants with various flow-velocities (exposure of heat source).

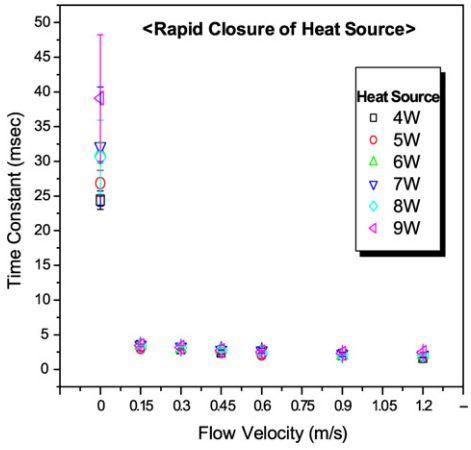

Fig. 13. Time constants with various flow-velocities (closure of heat source).

source. After the optical chopper intercepts the heat source, the periods of time when the temperature is decreased by the liquid are expressed as areas surrounded by the dash-dotted lines on the right-hand side of Fig. 14(b). The calculated results show that the algorithm developed in this study successfully distinguishes those regions in which temperature changes exist.

The comparisons of the two PDF transformed temperatures obtained from the original raw data and the data calculated by the developed algorithm are shown in Fig. 15. The PDF transformed temperatures obtained without the algorithm are determined directly from the raw data, which is well used in previous study. The PDF transformed temperatures determined with the algorithm are obtained by transforming the data, which are calculated by the algorithm developed in this study. The open symbols refer to the PDF transformed temperatures obtained from the raw data and the closed symbols refer to those obtained from the data calculated by the developed algorithm. T_{min} refers to liquid temperature and T_{max} refers to the temperature of the hot junction heated by the laser. Meanwhile, the measured temperature refers to the averaged liquid and laser beam temperature in the steady state, not undergoing temperature change due to the optical chopper.

The results show that the PDF transformed temperature obtained from the calculated data by means of the developed algorithm is more accurate than the PDF transformed temperature obtained directly from the raw data. According to the experimental results, the developed algorithm can distinguish phases and estimate each temperature quite accurately. 95% of data is within ±15% error. Also, even if the temperature of the hot junction does not reach the steady state, the algorithm more accurately estimates the temperature.

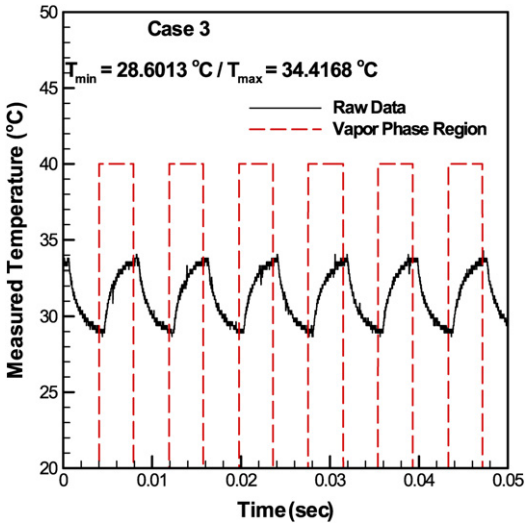

(a)

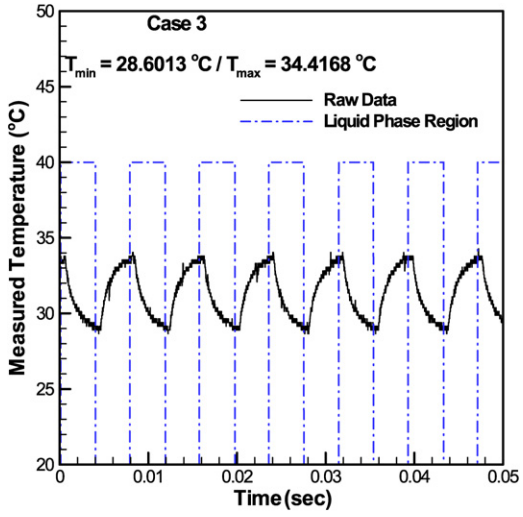

(b)

Fig. 14. Phase distinctions by the developed algorithm. (a) Vapor phase. (b) Liquid phase.

4.2. *Measurement of liquid temperature in subcooled boiling*

The subcooled boiling experiments have complex flow conditions, which are different from those in the experiments with the optical chopper. In the case of the experiment with the optical chopper, there were no liquid fluctuations. The liquid temperatures were determined as the peak temperatures in the temperature PDF. However, in this subcooled flow boiling, the changes in temperature are caused by the phase change and liquid fluctuations. For example, when the temperature is in-

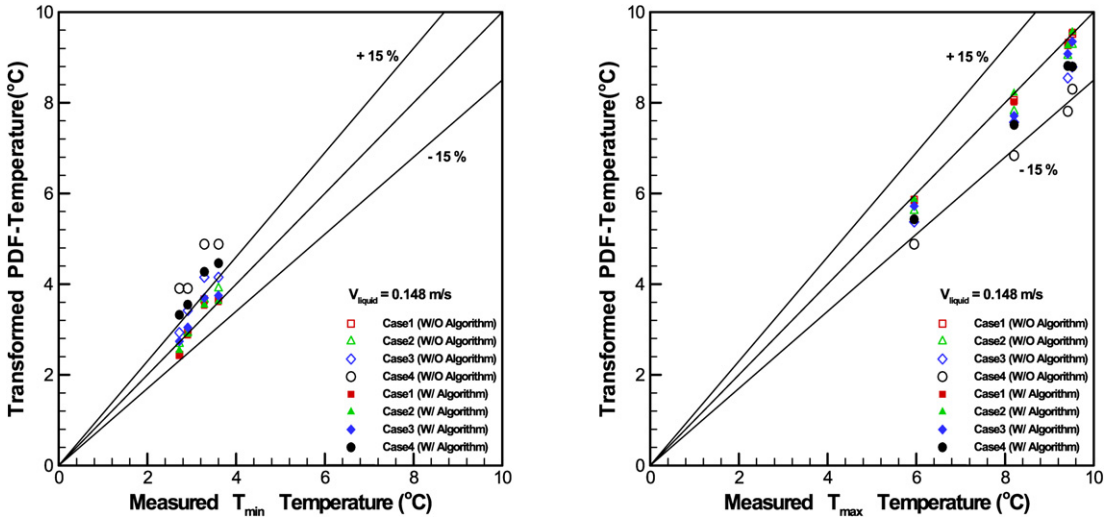

(a)

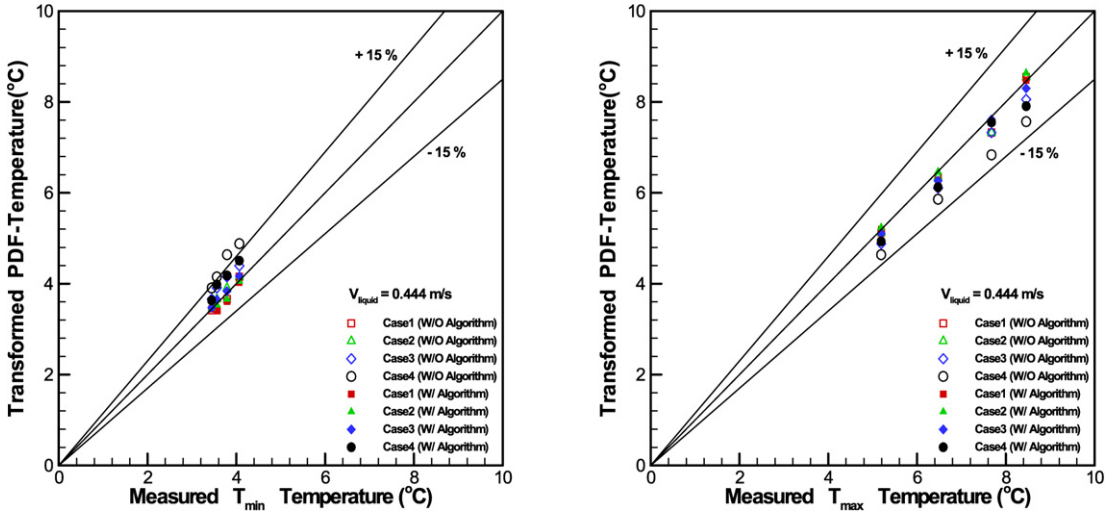

(b)

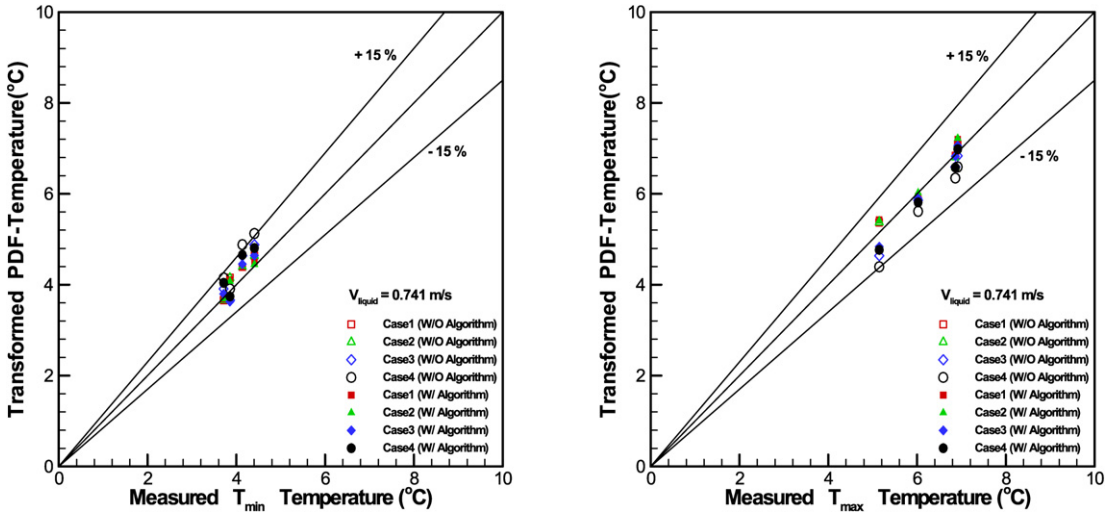

(c)

Fig. 15. (a) Comparison of measured and PDF transformed temperatures ($V_{\text{liquid}} = 0.148$ m/s). (b) Comparison of measured and PDF transformed temperatures ($V_{\text{liquid}} = 0.444$ m/s). (c) Comparison of measured and PDF transformed temperatures ($V_{\text{liquid}} = 0.741$ m/s). (d) Comparison of measured and PDF transformed temperatures ($V_{\text{liquid}} = 1.036$ m/s). (e) Comparison of measured and PDF transformed temperatures ($V_{\text{liquid}} = 1.332$ m/s).

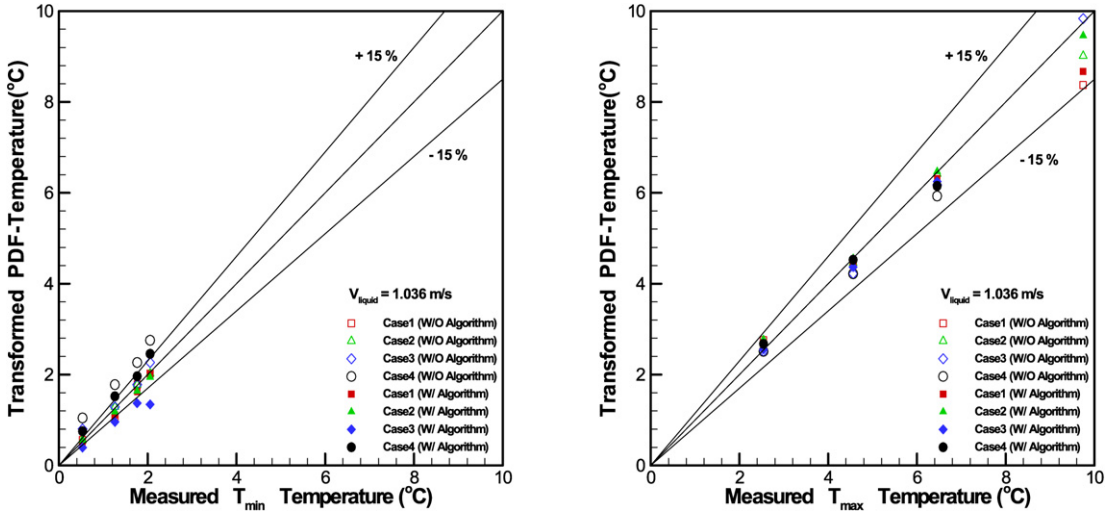

(d)

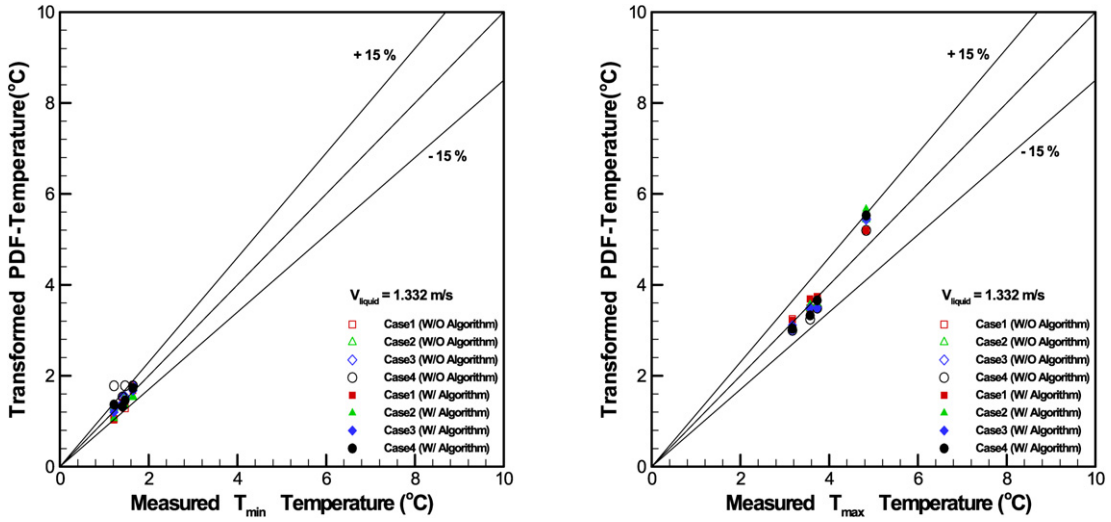

(e)

Fig. 15. (*Continued.*)

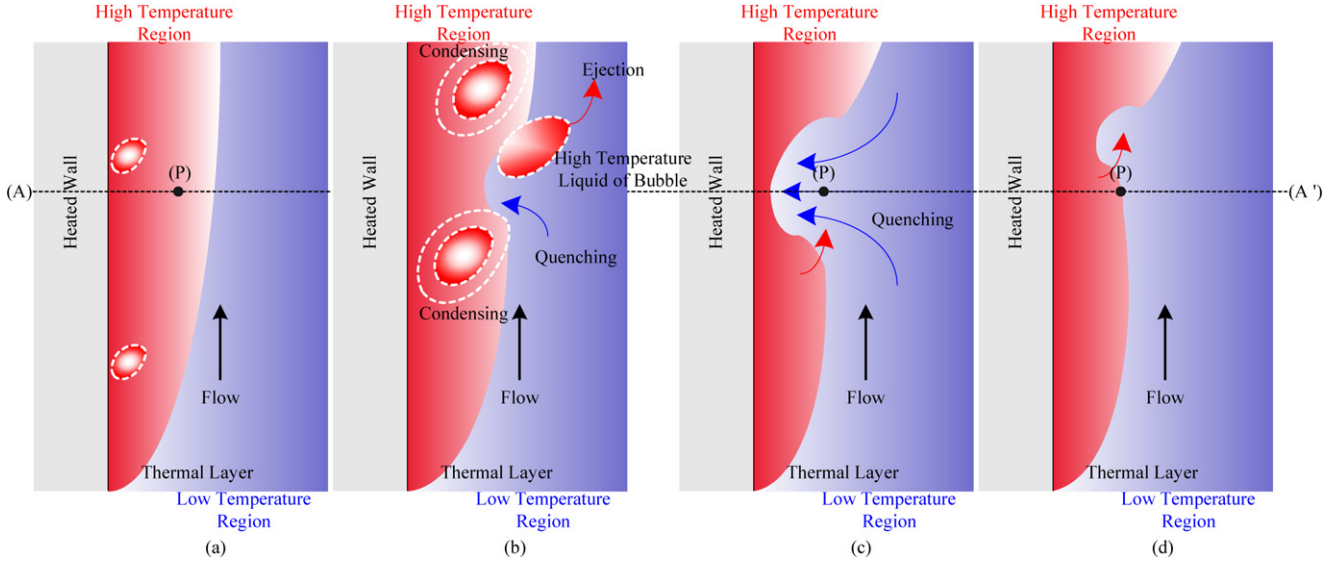

Fig. 16. Flow phenomena in subcooled region.

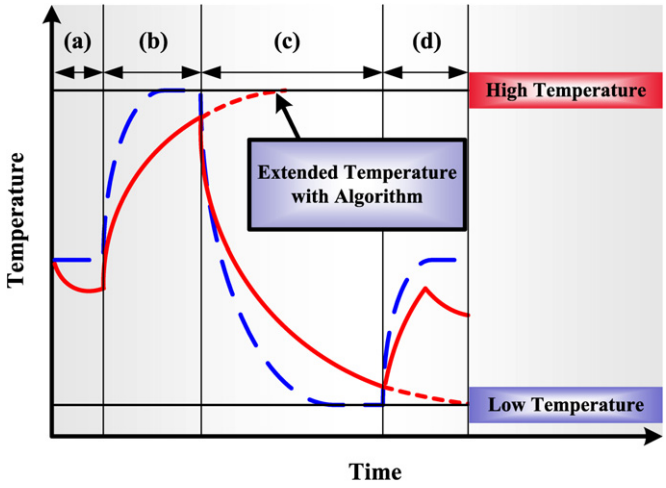

Fig. 17. Liquid temperature profile.

creased, the cause of the temperature change can be vapor passing through the hot junction or high temperature liquid passing through the junction due to liquid fluctuations. In contrast, the temperature is decreased by the phase change from vapor to low temperature liquid and by low temperature liquid inflowing into the hot junction, which is caused by the liquid fluctuation. Thus, the liquid temperatures are determined as the expectation values of the measured temperatures.

In the subcooled flow boiling, there are various fast and complex phenomena, which are caused by bubbles, and wakes that the bubbles invoke. In subcooled flow boiling, the liquid fluctuates due to the mixing of the liquid by convection and vapor condensation. The raw data for the temperature signals correspond to the direct temperature of the micro-thermocouple, which undergoes thermal change due to liquid fluctuations and phase changes. Thus, the raw temperature signals do not show the actual temperature changes, due to the problem of thermal. Fig. 16 shows these phenomena, schematically. The liquid is heated by bubble condensation and convection and is cooled by quenching of the bulk liquid, which is relatively cold. Fig. 17 shows the temperature trends at the point (P) on the line of (A)–(A′) in Fig. 16. The dashed line refers to the temperature when the residence time is longer than the time constant. In this case, the temperature can reach the convergent temperature. The solid line shows the case where the residence time is insufficient to reach the convergent temperature, such as in the general case. In this case, the micro-thermocouple undergoes thermal inertia. The convergent temperature can be found by means of the developed algorithm and is shown as the dotted line in Fig. 17. The raw data include not only the liquid temperature, but also the vapor temperature. Therefore, a distinction needs to be made between the liquid and vapor temperatures, which coexist in the raw data. The temperatures of raw data are divided into two temperatures, which are high and low temperature, when the developed algorithm is applied. The purpose of this division is to extract the major temperatures from the fluctuations of temperature present in the raw data. The high temperatures extracted by the algorithm refer to the major increase in temperatures of the liquid, while the low temperatures extracted

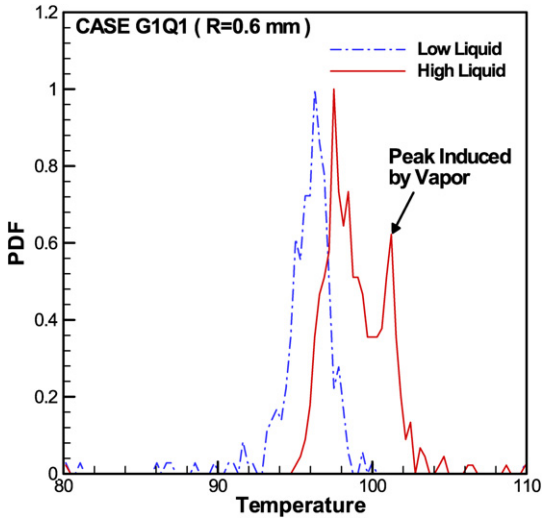

(a)

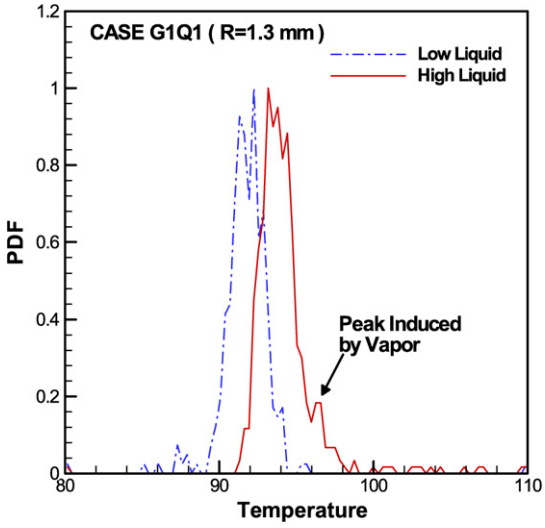

(b)

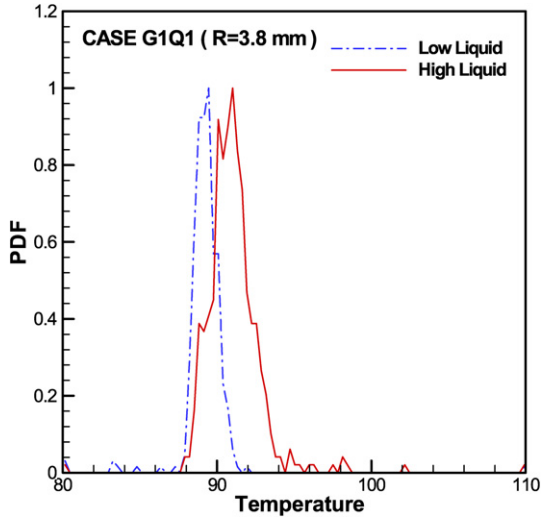

(c)

Fig. 18. (a) Temperature spectrum of liquid and vapor (case G1Q1, $R = 0.6$ mm). (b) Temperature spectrum of liquid and vapor (case G1Q1, $R = 1.3$ mm). (c) Temperature spectrum of liquid and vapor (case G1Q1, $R = 3.8$ mm).

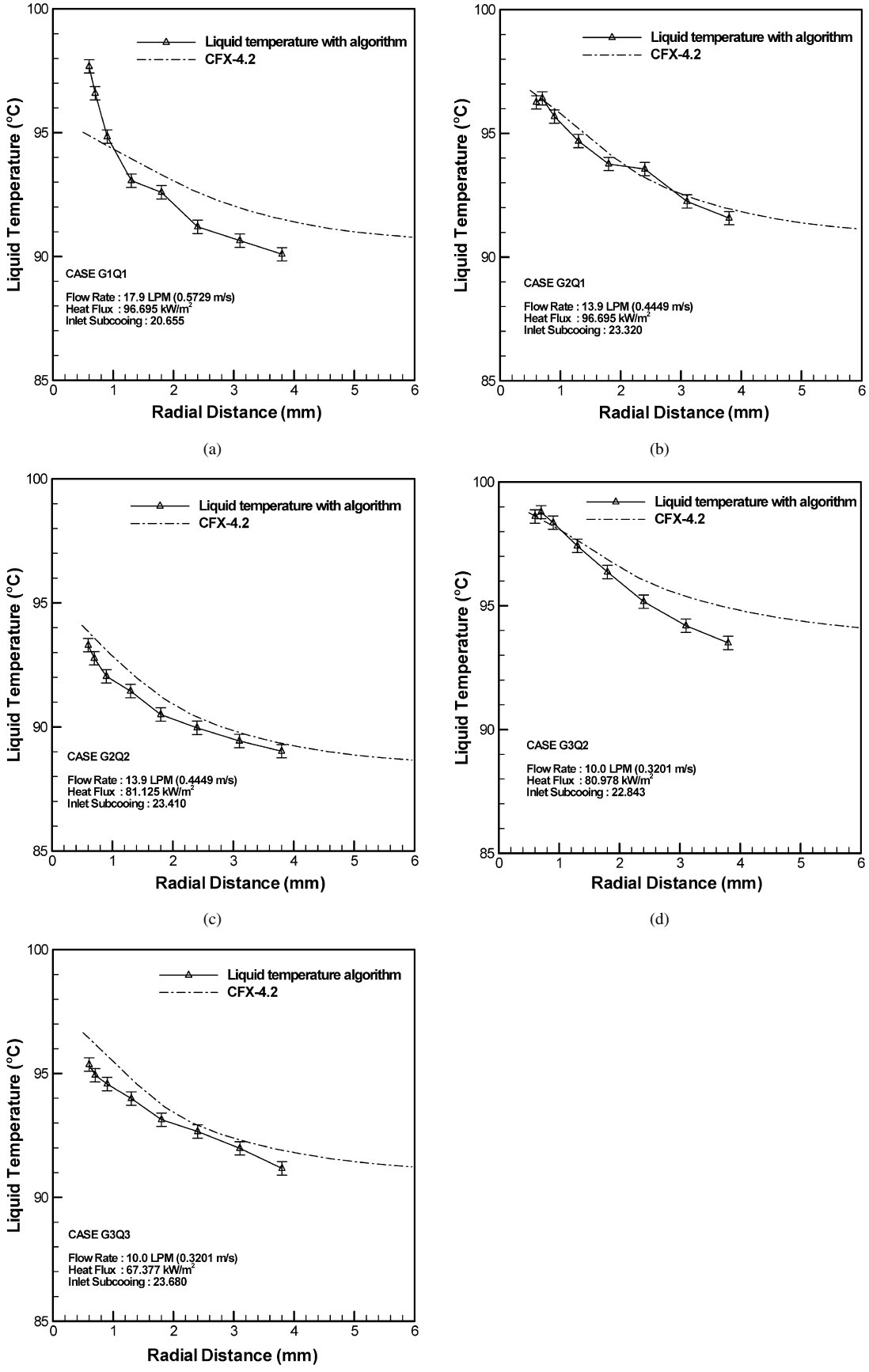

Fig. 19. Comparison of measured and calculated temperature. (a) Case G1Q1. (b) Case G2Q1. (c) Case G2Q2. (d) Case G3Q2. (e) Case G3Q3.

by the algorithm refer to the major decreases in temperatures of the liquid. The vapor temperatures are filtered using the difference in the time constants between the vapor and the liquid. The liquid temperature can be determined as the expectation value of the high and low temperatures.

The distinctions of low and high liquid temperature by the algorithm are depicted in Fig. 18. These figures are the results at the 0.6, 1.3, and 3.8 mm from the heated wall in case of G1Q1. In Fig. 18(a), the temperature peak induced by bubble is observed. However, as going far from the heated wall, the magnitude of the peak is smaller and then disappears in high-subcooled region as shown in Figs. 18(b) and (c). To measure local liquid temperature, purely, the portion of the vapor temperature is needed to eliminate. Thus, the pure temperature portions by liquid are considered in raw data with the algorithm using differences of time constants between liquid and vapor. In addition, the representative temperatures of low and high liquid region in the local position are found with the algorithm. The obtained temperature of the low and high liquid temperature used to determine the liquid temperatures as the expectation values

The liquid temperature estimated by the algorithm and the results of CFX-4.2 code are plotted in Fig. 19 with error bars. The triangle symbols in Fig. 19 refer to the estimated liquid temperature obtained with the developed algorithm. The dash-dotted line shows the results obtained with CFX-4.2. In Fig. 19 the results obtained with CFX-4.2 show that the liquid temperatures are a little overestimated, as the distance from the heated wall is going far away. However, the calculated temperature with CFX-4.2 show comparatively good agreement with the estimated temperatures obtained using the developed algorithm.

The decline gradient of temperature in CFX is gentler than experiments and this means that CFX has the higher thermal mixing by turbulence. For a high liquid velocity, the most of bubble condensation occurs near the heater and the thermal boundary layer is thinner as the liquid velocity increases. Thus the temperature gradient is steeper. From experimental results, the liquid temperature gradient in the direction of the heater increased rapidly as the liquid velocity increases. However, CFX-4.2 does not follow those trends, which is suggested from the weakness of wall temperature calculation capability of CFX.

5. Conclusion

In this study, a micro-thermocouple having a diameter of 12.7 μm was fabricated and an algorithm was developed to estimate the temperature of each phase, when phase changes exist at the hot junction of the micro-thermocouple. The response time of the micro-thermocouple is measured by dynamic calibration and it was shown to be of the order of several milliseconds. The newly proposed algorithm was verified by conducting experiments simulating phase changes using an optical chopper and laser. According to the experimental results, the developed algorithm estimate 95% of temperature data within ±15% error.

The fabricated micro-thermocouple and the developed algorithm were used to measure the liquid temperature in subcooled flow boiling. In this study, the fluctuation and phase change could be measured using the fabricated micro-thermocouple. The temperature was classified into the major temperatures needing to be compensated using the developed algorithm, except in the case of the vapor temperature. The estimated liquid temperature to be the expectation value for the extracted temperatures applying the developed algorithm compared with the CFX-4.2 code. The results showed the CFX-4.2 made a good agreement with the estimated liquid temperature, comparatively. However, the calculated result didn't follow the rapid increased trends of liquid temperature when the liquid velocity increased. This shows the necessity of improving subcooled boiling model in CFX-4.2 code.

References

[1] L.M. Jiji, J.A. Clark, Bubble boundary layer and temperature profiles for forced convection boiling in channel flow, Journal of Heat Transfer 86 (1964) 50–58.

[2] G.E. Walmet, F.W. Staub, Pressure, temperature, and void fraction measurement in nonequilibrium two-phase flow, in: Two-Phase Flow Instrumentation, Eleventh National Heat Transfer Conference, A.I.Ch.E.–A.S.M.E., Minneapolis, MN, 1969, pp. 89–101.

[3] J.M. Delhaye, R. Semeria, J.C. Flamand, Void fraction and vapor and liquid temperature: Local measurements in two-phase flow using a microthermocouple, Journal of Heat Transfer 95 (1973) 365–370.

[4] A. Hasan, R.P. Roy, S.P. Kalra, Some measurements in subcooled flow boiling of refrigerant-113, Transactions of the ASME 113 (1991) 216–223.

[5] P. Beckman, R.P. Roy, K. Whitfield, A. Hasan, A fast-response microthermocouple, Review of Scientific Instrumentation 64 (1993) 2947–2951.

[6] R.P. Roy, V. Velidandla, S.P. Kalra, P. Peturaud, Local measurements in the two-phase region of turbulent subcooled boiling flow, Transactions of the ASME 116 (1994) 660–669.

[7] P. Beckman, R.P. Roy, V. Velidandla, M. Capizzani, An improved fast-response microthermocouple, Review of Scientific Instrumentation 66 (1995) 4731–4733.

[8] H. Nakamura, T. Igarashi, T. Tsutsui, Local heat transfer around a wall-mounted cube in the turbulent boundary layer, International Journal of Heat and Mass Transfer 44 (2001) 3385–3395.

[9] G.R. Warrier, N. Basu, V.K. Dhir, Interfacial heat transfer during subcooled flow boiling, International Heat and Mass Transfer 45 (2002) 3947–3959.

[10] S.F.J. Langer, Efficient exponential regression with exact fiducial limits to fit cardiac pressure data, Computer Methods and Programs in Biomedicine 53 (1997) 57–64.